Supporting Information

Simple Additive Strategy to Boost Initial Coulombic Efficiency by Mitigating PTFE Decomposition in Dry Battery Electrodes

Hyunji Park[1] *and Choongho Yu*[1,2*]

[1] Department of Mechanical Engineering

[2] Department of Materials Science and Engineering

Texas A&M University, College Station, Texas 77843 USA

*Corresponding author: chyu@tamu.edu

Experimental Section

Density functional theory (DFT) calculations

The DFT calculations were carried out with the ORCA 4.2.1 computational package. (*1, 2*) For geometry optimization, B3LYP functional coupled with the def2/TZVPP basis set were employed and the auxiliary basis sets def2/J and def2-SVP/C were used. Converged self-consistent field orbitals were obtained using the normal setting in ORCA. For the molecular modeling and visualization, Avogadro 1.2.0 was used. The binding energies (E_b) between polytetrafluoroethylene (PTFE) and additives were calculated using the following formula.

$$E_b = E_{total} - E_{PTFE} - E_{add}$$

Where E_{total} is the energy of the configuration of the additive absorbed on PTFE; E_{PTFE} and E_{add} are the energies of PTFE and additive, respectively.

Preparation of dry-processed electrodes with PTFE binder and additives

PTFE powder was obtained after removing the remaining surfactant of PTFE preparation (60 wt % dispersion in H_2O, Sigma Aldrich) by stirring in deionized water at 70 ℃ for a day and rinsing several times with water. PTFE is mixed with Tyramine (Ty, > 98.0 %, Sigma Aldrich) using a chopper at a ratio of 5:1 or 2:1 wt%, and then mixed with mortar and pestle to break Ty into smaller pieces by applying shear force for maximizing interaction between Ty and PTFE. To ensure sufficient dispersion of Tyramine, the film chopping and shear mixing processes were repeated five times (Figure S1). The natural graphite (MSE Supplies) and artificial graphite (Xiamen TOB New Energy Tech)) electrodes were prepared with PTFE@Ty by applying shear force using mortar and pestle until mechanically robust films were obtained. According to the manufacturer's

specifications, the natural graphite exhibits an initial Coulombic efficiency of 95%, a median particle size (D50) of 17-19 μm, and a specific surface area of 2-3 $m^2 g^{-1}$, whereas the artificial graphite shows an initial Coulombic efficiency of 94.6%, with a D50 of 14 μm and a specific surface area of 1.888 $m^2 g^{-1}$. The dry-processed electrodes for half cells were fabricated with natural graphite and binder (without additive) at a weight ratio of 98:2. With the additive, the ratio of graphite, binder, and additive was 97.6:2:0.4. The dry-processed anodes for full cells without the additive in Figure 4 and 5, carbon nanotubes (CNT, Carbon Nano-material Technology Co., Ltd.) were added with weight ratios of 96:2:2 (artificial graphite: CNT: binder). When the additive was incorporated, the ratio of PTFE to the conductive agent was kept constant, and the active material content was reduced accordingly. For example, in the case of PTFE@Ty (2:1 wt%), the ratio of graphite, CNT, binder, and additive was 95:2:2:1.

The dry-processed films were spread to desired thicknesses and loadings using a hand roller, and then cut into a circular shape using a 3/8-inch diameter punch. The thickness, electrode density, and mass loading of dry-processed anodes with an areal capacity of 4.4 mAh cm^{-2} were approximately 80 μm, 1.4 g cm^{-3}, and 12.6 mg cm^{-2}, respectively. An additional adhesive layer was applied to the Cu current collector to improve the adhesion between the freestanding dry-processed film and the current collector to provide conditions similar to those used in the wet process for fair comparison. (*3*) The adhesive was prepared by mixing polyvinylidene fluoride (PVDF, Mw ~534,000, Sigma Aldrich) and carbon black (Super P, MSE Supplies) in N-methyl-1,2-pyrrolidine (NMP, Sigma Aldrich) with a weight ratio of PVDF:Super P = 3:2, and a solid content of 5 wt%. The adhesive layer was uniformly coated on the copper current collector using a doctor blade. The dry electrode was placed on the adhesive layer and dried in an oven at 60 °C

for 6 hours.

Assembly and test of the coin cells

The coin cell was assembled with a CR2025 battery casing. A carbonate-based electrolyte for half cells and full cells used in Figure 3 was prepared by dissolving 1.0 M lithium hexafluorophosphate ($LiPF_6$) (≥99.99%, Sigma Aldrich) and 0.05 M lithium difluoro(oxalate)borate (LiDFOB) (95.0%, AmBeed) in a solution of ethyl methyl carbonate (EMC, 99.9%, Sigma Aldrich) and 4-fluoro-1,3-dioxolan2-one (fluoroethylene carbonate or FEC, >98.0 %, TCI) with a volume ratio of 3:1. (*4*) The half cells were assembled with 65-µm-thick lithium foils and Al_2O_3 coated polyethylene separators (Mirong), and charged using constant current-constant voltage (CC-CV) charging mode for cycling (0.1C cut-off). The wet-processed $LiNi_{0.8}Mn_{0.1}Co_{0.1}O_2$ (NMC811) cathode with an areal capacity of 4.0 mAh cm^{-2} (Custom-made Nanomute BE-56E, NEI Corp.) has a total loading of 23.18 mg cm^{-2} and a total active material loading of 20.86 mg cm^{-2} (±0.2 mg cm^{-2}). The cathode was fabricated with a weight ratio of 90:5:5 for the active material, Super P, and PVDF. For the wet-processed anode, the CMC/SBR binder was prepared by mixing carboxymethylcellulose (CMC, high viscosity, EMD Millipore Corp.) and styrene-butadiene rubber (SBR, MTI Corp.) at a 1:1 weight ratio. Water was used as a solvent with a solid content of 30 wt%. The slurry was applied onto a copper foil using a doctor blade, and then dried overnight at 60 °C. The electrode was densified using a calendaring machine to obtain an electrode density similar to that of the dry-processed electrodes. In the full cells used in Figure 4 and Figure 5, the electrolyte was prepared by mixing 1.2 M $LiPF_6$ in a 95:5 volume ratio of EMC:FEC, along with 1% vinylene carbonate (VC) and 0.5% LiDFOB. The N/P ratio was 1.1 and CC-CV charging mode (0.1C cut-off) for cycling. All battery tests were run at room temperature with Neware battery cyclers.

Materials Characterization

The Fourier transform infrared (FT-IR) spectroscopy analysis was performed using Thermo Nicolet 380 FT-IR spectrometer. The scanning electron microscope (SEM) images were taken with a JEOL JSM-7500F filed-emission scanning electron microscope. The X-ray photoelectron spectroscopy (XPS) and ultraviolet photoelectron spectroscopy (UPS) were carried out with an Omicron XPS/UPS system with DAR 400 dual Mg/Al X-ray source (< 5×10^{-9} Torr condition) for XPS measurements and HIS 13 emitting at 21.2 eV (He I radiation) for UPS measurements. The XPS results in Figure 2(d,e) were obtained from composites consisting of 95 wt% copper powders (99% trace metal basis, BTC) and 5 wt% binder (either PTFE or PTFE@Ty (5:1)). The binders were mixed with copper powders to avoid charging effects. UPS was measured by compressing the PTFE film onto copper foil using a heated calendaring machine. The Ultraviolet-Visible (UV-Vis) spectra were obtained using Hitachi U-4100 UV-Vis-NIR Spectrophotometer.

The galvanostatic intermittent titration technique (GITT) was performed at 0.05C (2 mA cm^{-2}) with a 10-min charge interval and a 1-h rest protocol. GITT was conducted using an anode with an areal capacity of 4 mAh cm^{-2}, with one of the three different artificial graphite anodes: dry-processed with a PTFE (2 wt%) binder, dry-processed with a PTFE@Ty (2,1 wt%) binder, or wet-processed with a CMC/SBR (2 wt%) binder. The anodes contained 2 wt% CNT, and the electrolyte used was 1M $LiPF_6$ in EMC:FEC (3:1 vol%) with 0.5 wt% LiDFOB. The calculated lithium-ion diffusion coefficient from the GITT results was obtained using the formula $D_{Li^+} = \frac{4}{\pi\tau}\left(\frac{m_B V_M}{M_B S}\right)^2 \left(\frac{\Delta E_S}{\Delta E_\tau}\right)^2$ where τ is the constant current pulse time (600s), m_B is the mass of active material, V_M is the molar volume of the electrode (5.3 cm^3 mol^{-1}), M_B is molecular weight of the

active material (12.01 g mol^{-1}), S is the surface area of the electrode (0.71 cm^2), ΔE_s is the change of the steady-state voltage during a single-step test, and ΔE_τ is the total change of cell voltage during a constant current pulse of a single-step. (*5, 6*) Electrochemical impedance spectroscopy (EIS) analysis was performed with an Arbin battery analyzer connected with a Gamry tester over a frequency range of 0.01 Hz –1 MHz with a voltage perturbation of 5 mV. EIS was measured using a symmetric cell with anodes prepared with PTFE (2 wt%), PTFE@Ty (2,1 wt%), or CMC/SBR (2 wt%) binders. The anodes for symmetric cells contained 2 wt% CNT, and the electrolyte used was 1M $LiPF_6$ in EMC:FEC (3:1 vol%) with 0.5 wt% LiDFOB.

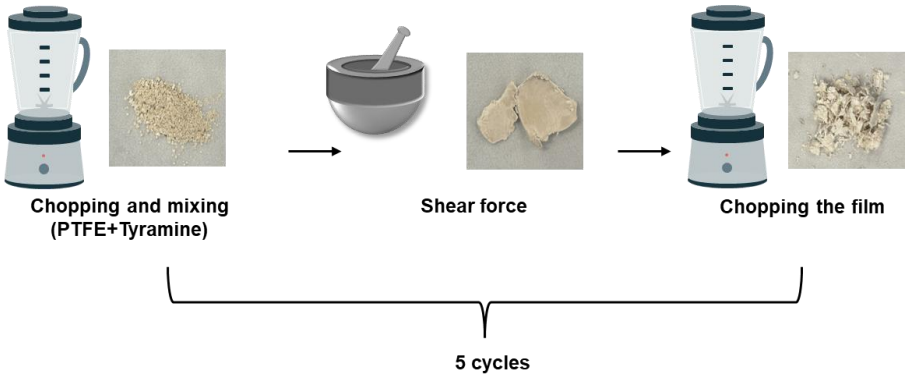

Figure S1. Schematic illustration of the repeated film-chopping and shear-mixing process used to ensure uniform dispersion of Tyramine within the PTFE matrix.

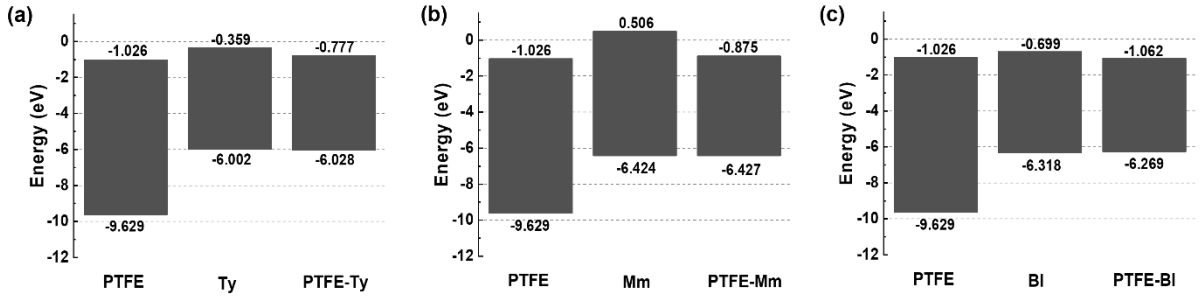

Figure S2. Calculated energy level diagrams of PTFE and additives of (a) tyramine (Ty), (b) melamine (Mm), and (c) benzimidazole (BI).

Table S1. The DFT results of PTFE, additives, and complexes.

	PTFE	Ty	PTFE-Ty	Mm	PTFE-Mm	BI	PTFE-BI
Total energy [Eh]	-2102.092	-441.3521	-2543.450	-446.4449	-2548.540	-379.7841	-2481.880

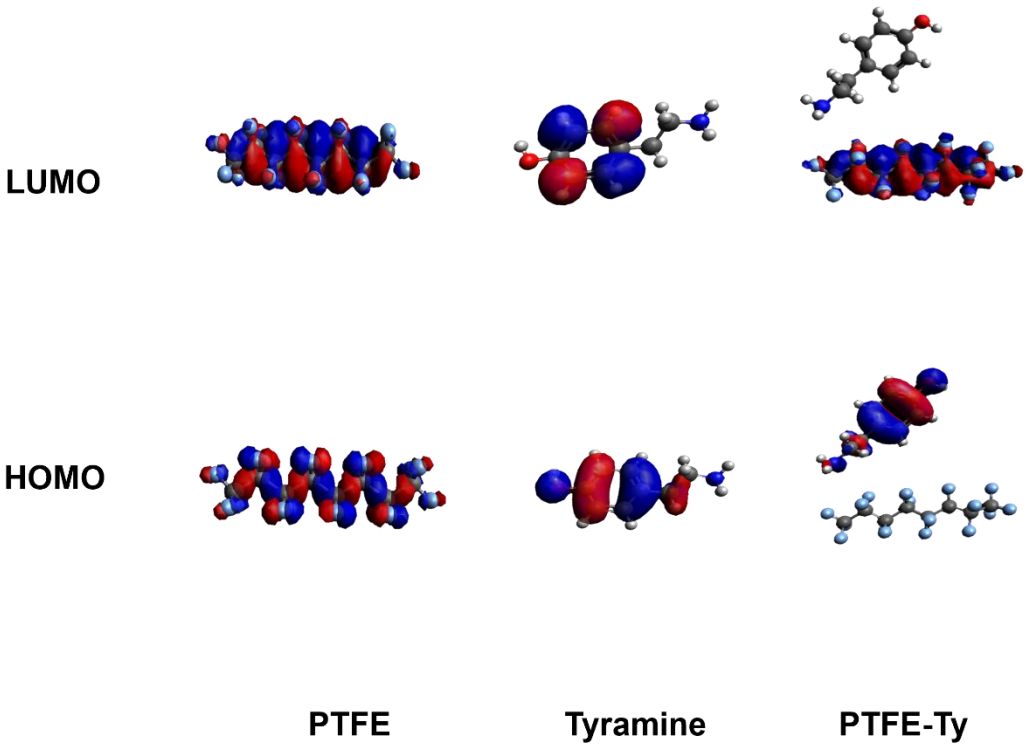

Figure S3. The electron density distributions of the lowest unoccupied molecular orbital (LUMO) and highest occupied molecular orbital (HOMO) for PTFE, tyramine, and PTFE-Ty.

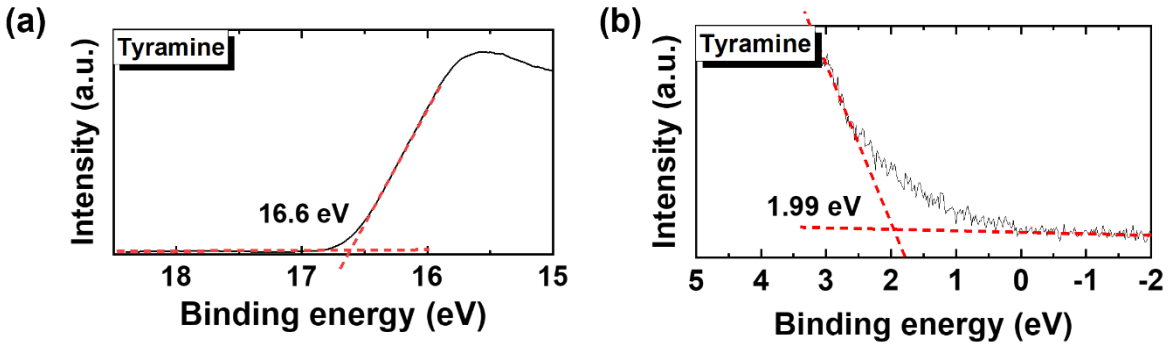

Figure S4. UPS spectra of tyramine: (a) cut-off region and (b) onset region. Tyramine was coated thinly onto copper foil at a concentration of 1 mg mL^{-1} in ethanol, then dried overnight in a 60 °C oven before conducting UPS measurements.

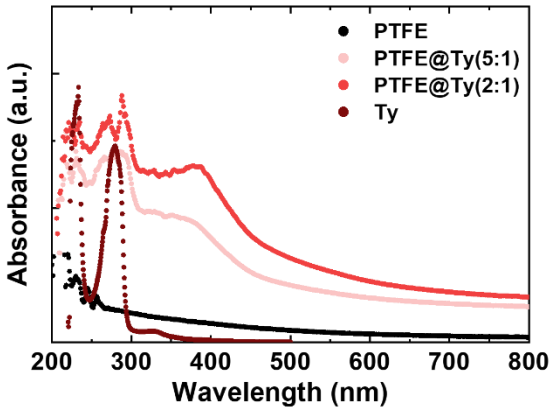

Figure S5. UV-Vis absorbance spectra of PTFE, tyramine, and PTFE@Ty. PTFE and PTFE@Ty were measured as thin films with a thickness of 100 μm, while tyramine was dissolved in ethanol at a concentration of 1 mg mL^{-1} for the measurement.

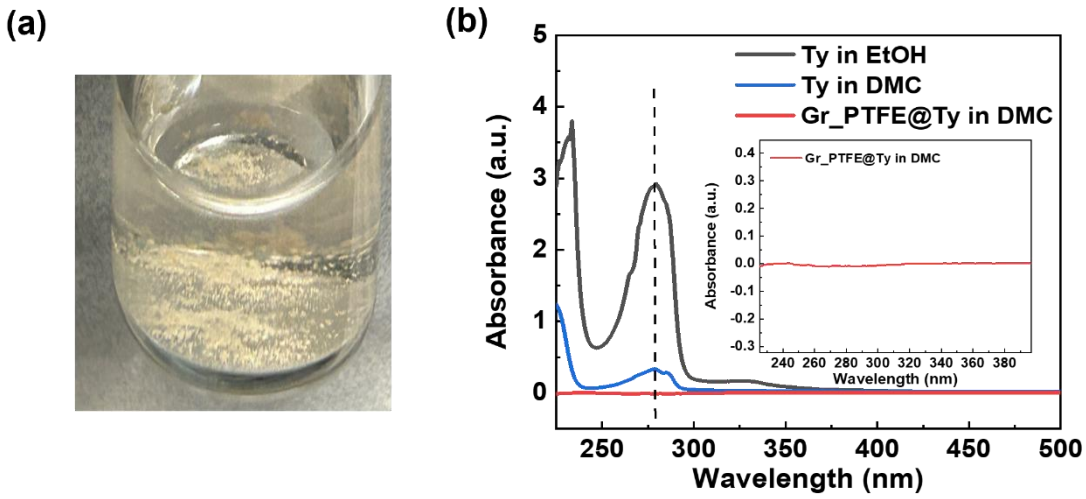

Figure S6. Tyramine solubility test: (a) Photo of tyramine in a 1 mg mL^{-1} carbonate-based solvent. (b) UV-Vis absorbance spectra of tyramine in ethanol and dimethyl carbonate (DMC) (inset: an electrode with tyramine in DMC). Using Beer's Law, the molar absorptivity (ε) in ethanol was calculated to be 2.9×10^4 M^{-1} cm^{-1}. In DMC, the measured absorbance of 0.32 corresponds to a concentration of 1.03×10^{-5} mol L^{-1} (0.00137 mg mL^{-1}), indicating the low solubility of tyramine. After interacting with PTFE and graphite in the film, the amount of dissolved tyramine, if any, is very low.

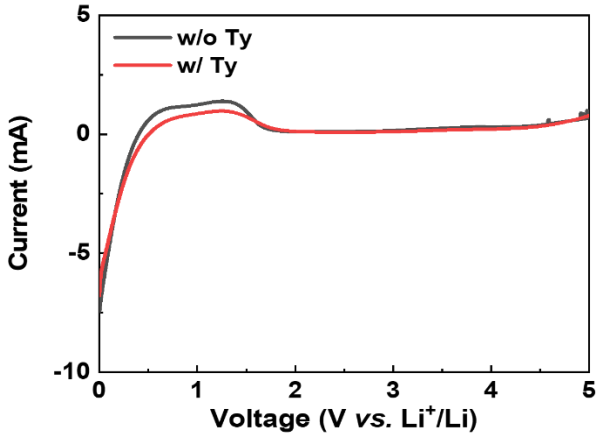

Figure S7. Linear sweep voltammetry **(**LSV) curves of electrodes with and without tyramine in a half-cell configuration at a sweep rate of 1 mV s^{-1}. The two different types of electrodes were made of tyramine, carbon black, and PVDF whose weight ratios are 60:30:10 (with tyramine) or 0:90:10 (without tyramine). The electrodes were fabricated using a wet slurry process with NMP onto an aluminum current collector with a doctor blade. PVDF was used instead of PTFE to avoid PTFE peaks, as the LSV measurement aimed to assess the electrochemical stability of Tyramine itself. A carbonate-based electrolyte was prepared by dissolving 1.0 M $LiPF_6$ and 0.05 M LiDFOB in a mixture of EMC and FEC with a volume ratio of 3:1.

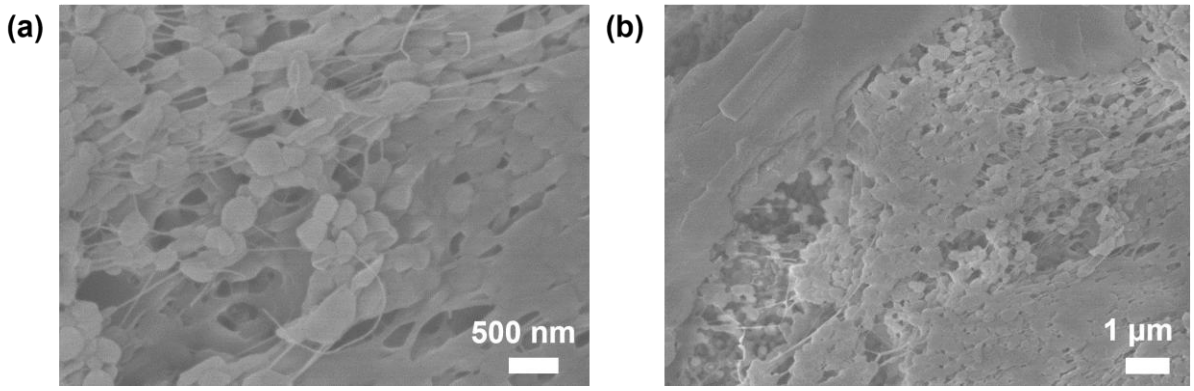

Figure S8. SEM images of pristine PTFE.

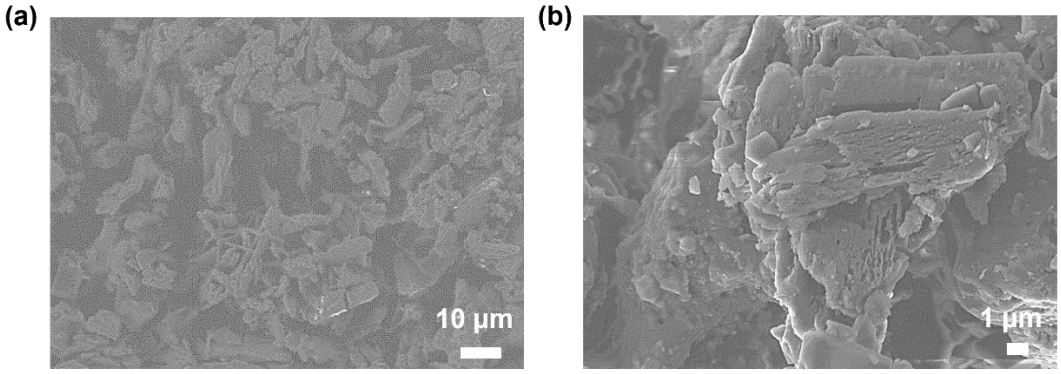

Figure S9. SEM image of tyramine particles.

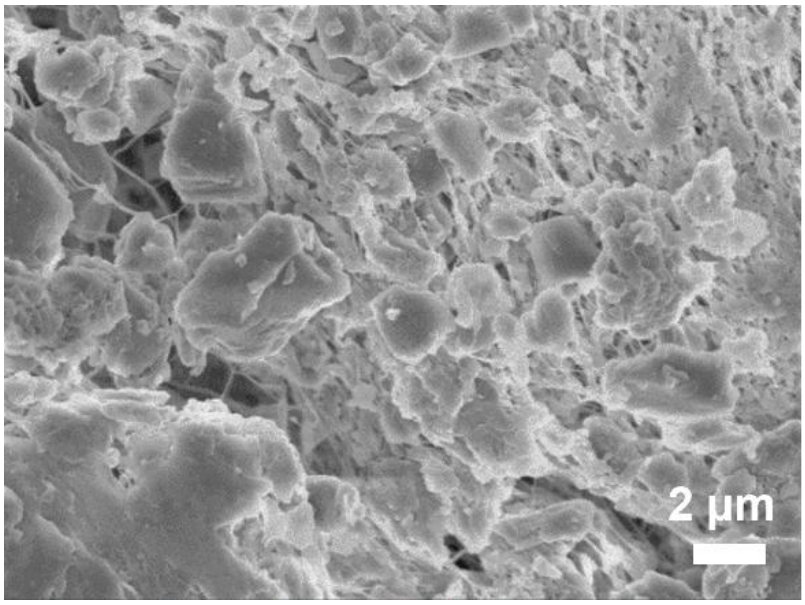

Figure S10. SEM image of PTFE@Ty. The ratio of PTFE to Ty was 5:1. The weight ratio of PTFE to Ty was 5:1. The PTFE and Ty were mixed by using a chopper and then applying shear force with a mortar and pestle. This mixing process was repeated five times to obtain the PTFE@Ty binder.

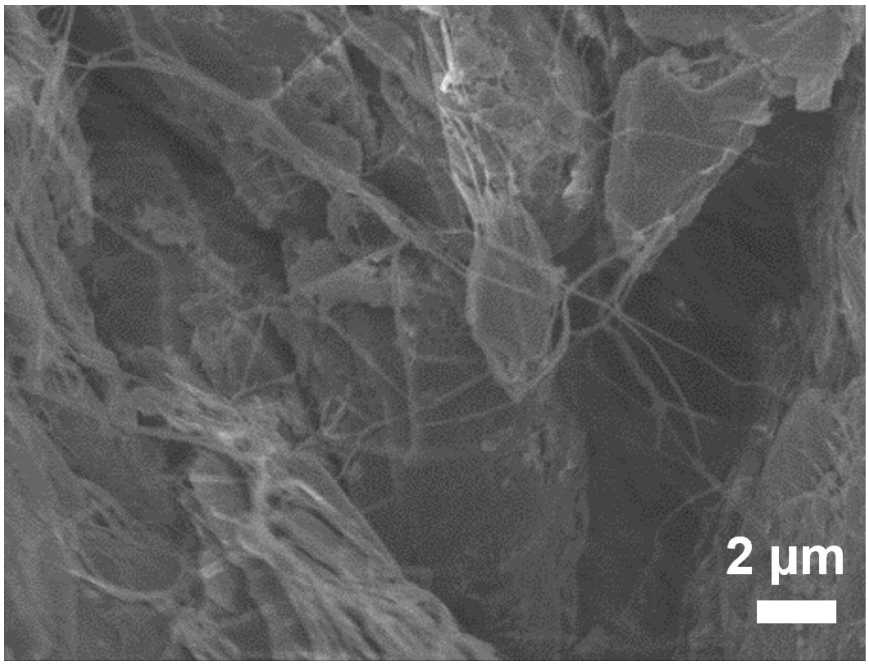

Figure S11. SEM image of the natural graphite electrode with PTFE binder. The ratio of graphite to PTFE was 95:5 wt%.

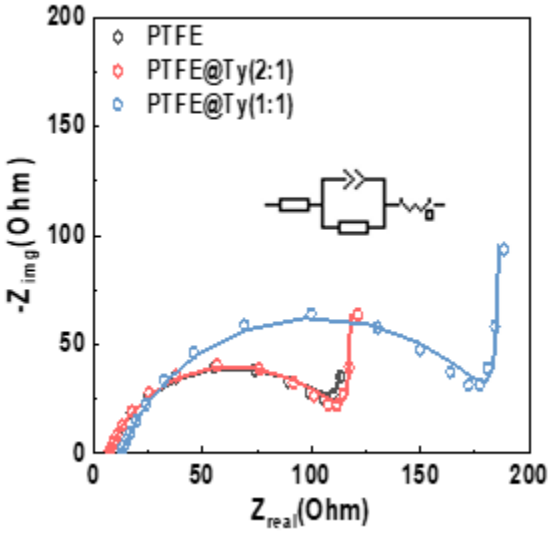

Figure S12. Electrochemical impedance spectra (EIS) of PTFE, PTFE@Ty (2:1), and PTFE@Ty (1:1) half-cells measured prior to cycling. Open circles represent the experimental data, and solid lines correspond to the fitted data using the equivalent circuit shown in the inset.

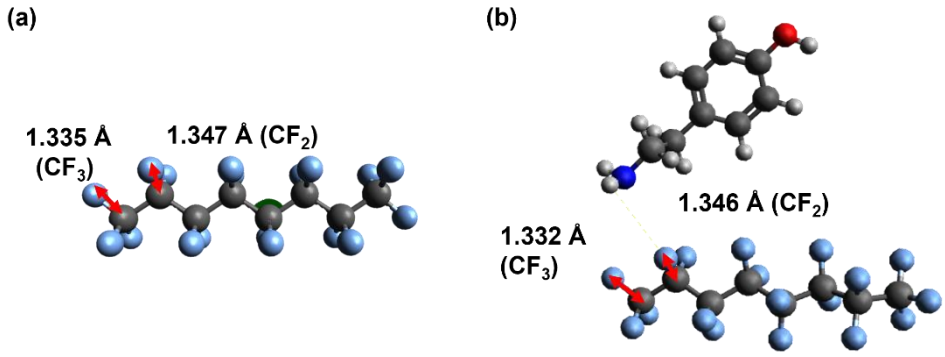

Figure S13. The bond length between carbon and fluorine (a) before and (b) after the formation of hydrogen bonding in PTFE, as calculated by DFT.

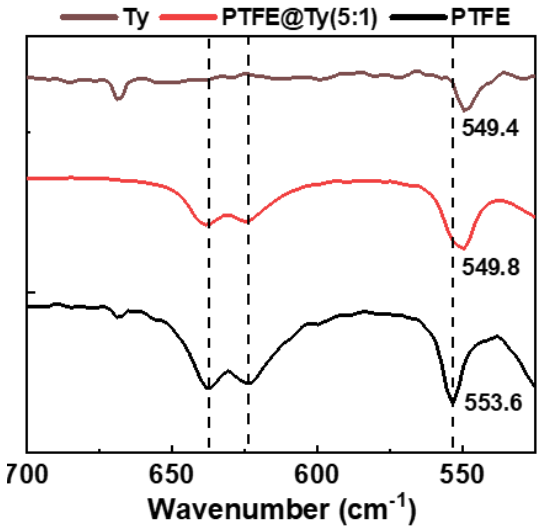

Figure S14. FT-IR spectra of wagging and bending vibrations of C-F_2. The bending vibration peak of C-F_2 in PTFE is at 553.6 cm^{-1}, but it overlaps with the 549.4 cm^{-1} peak of Ty, making it difficult to identify if the composite has blue or red shift.

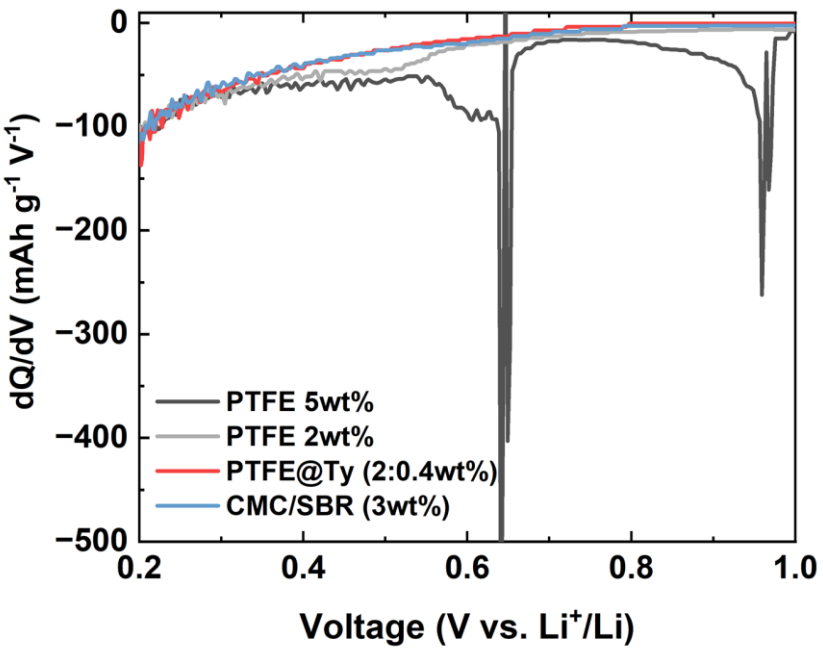

Figure S15. Differential capacity (dQ/dV) analysis of voltage profiles during the initial lithiation, as derived from Figure 3(a).

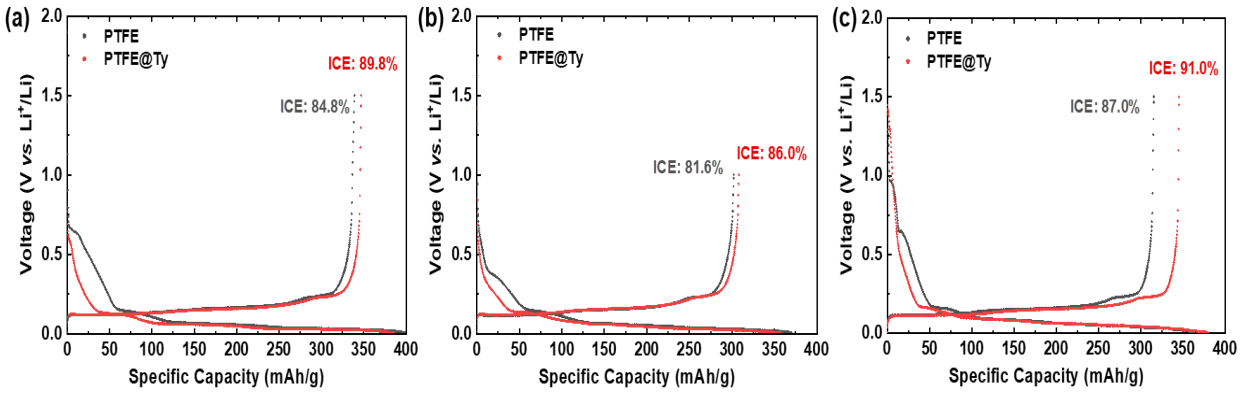

Figure S16. Initial charge/discharge profiles in various electrolytes: (a) 1.2M $LiPF_6$ in ethylene carbonate (EC):EMC (3:7 vol%) (b) 1.15M $LiPF_6$ in EC:EMC:dimethyl carbonate (DMC) (2:4:4 vol%) with 1.5% VC and 1% LiDFOB (c) 1M $LiPF_6$ in EMC:FEC (3:1 vol%) with 0.5 M LiDFOB.

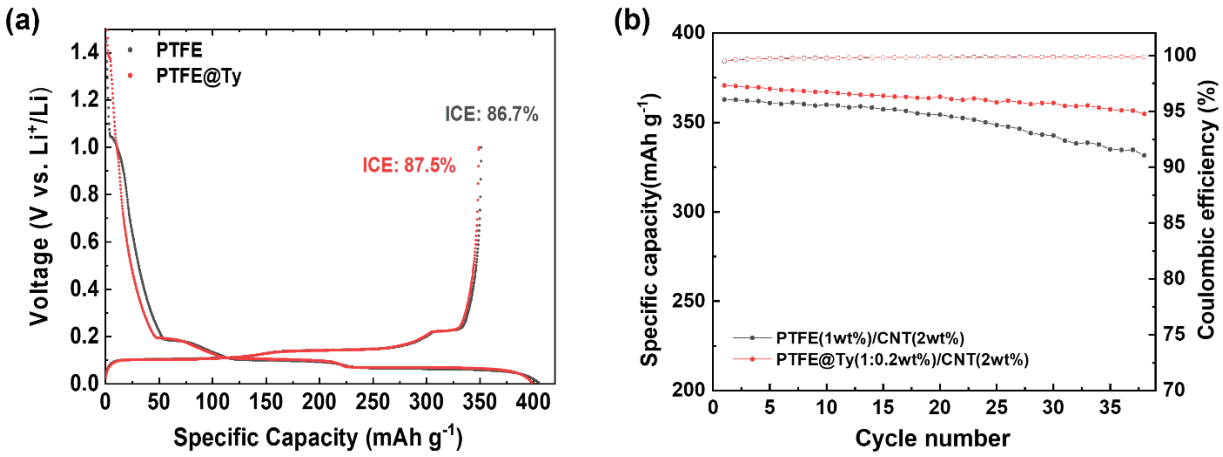

Figure S17. (a) The first charge/discharge curve and the initial Coulombic efficiency (ICE) of the half cells containing CNT at 0.05C in comparison to the half cells without CNT in Figure 3(c). For the PTFE electrode, the ratio of natural graphite, CNT, PTFE, and Ty is 97:2:1:0, while for PTFE@Ty, the ratio is 96.8:2:1:0.2. (b) Cycle performances of the half cells at 0.3C with 1 wt% PTFE, comparing the presence and absence of CNT. The electrolyte consists of 1.0 M $LiPF_6$ and 0.5 M LiDFOB in a solution of EMC and FEC with a volume ratio of 3:1.

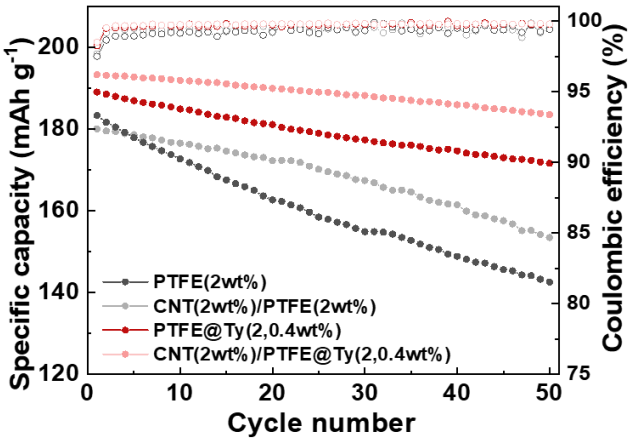

Figure S18. Specific capacity and Coulombic efficiency of full cells shown in Figure 3(d) as a function of cycle at 0.3C. The electrolyte consists of 1.0 M $LiPF_6$ and 0.5 M LiDFOB in a solution of EMC and FEC with a volume ratio of 3:1.

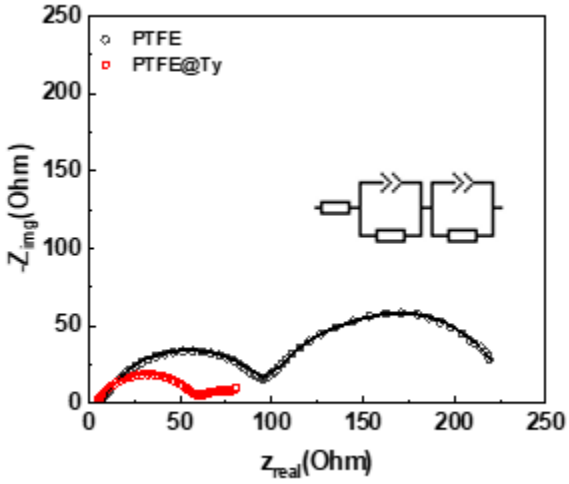

Figure S19. Nyquist plots of half cells after formation cycling. The inset shows the equivalent circuit used for fitting; open circles represent the measured data, and solid lines correspond to the fitted data.

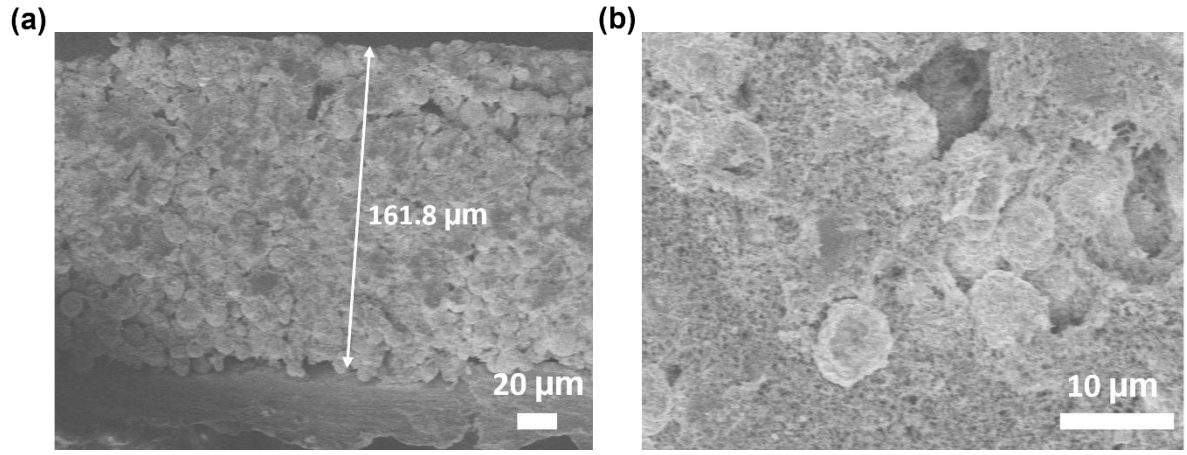

Figure S20. (a) Cross-sectional and (b) top-view SEM images of the wet-processed pristine NMC 811 cathode before cycling.

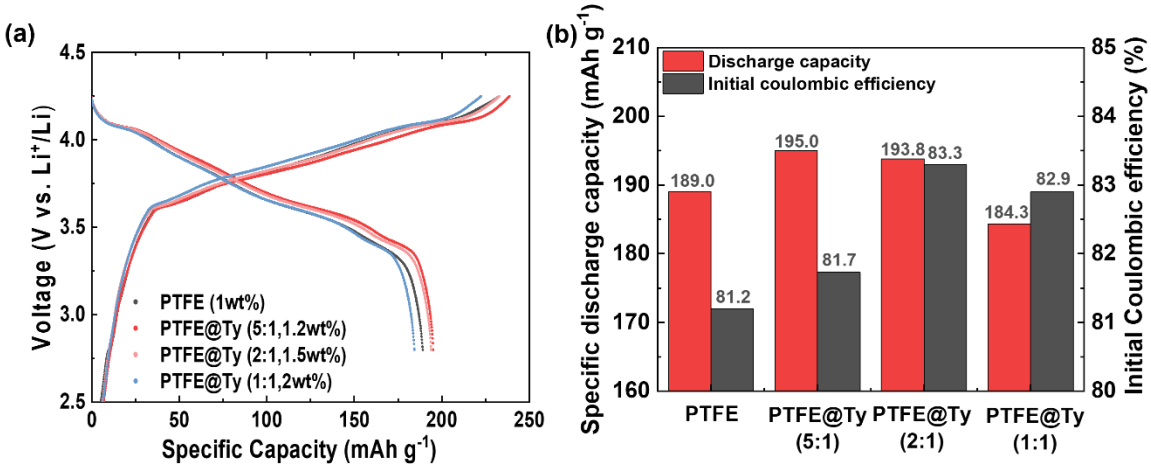

Figure S21. (a) First charge/discharge curves and (b) comparison of the first discharge capacity and ICE based on the ratio of PTFE to Ty for the full cells made of $LiNi_{0.8}Mn_{0.1}Co_{0.1}O_2$ cathode and natural graphite anode at 0.05C. The composition wt% ratios of graphite:CNT:PTFE:Ty are as follows: 97:2:1:0 for PTFE; 96.8:2:1:0.2 for PTFE@Ty (5:1); 96.5:2:1:0.5 for PTFE@Ty (2:1); and 96:2:1:1 for PTFE@Ty (1:1). The electrolyte consists of 1.0 M $LiPF_6$ and 0.5 M LiDFOB in a solution of EMC and FEC with a volume ratio of 3:1.

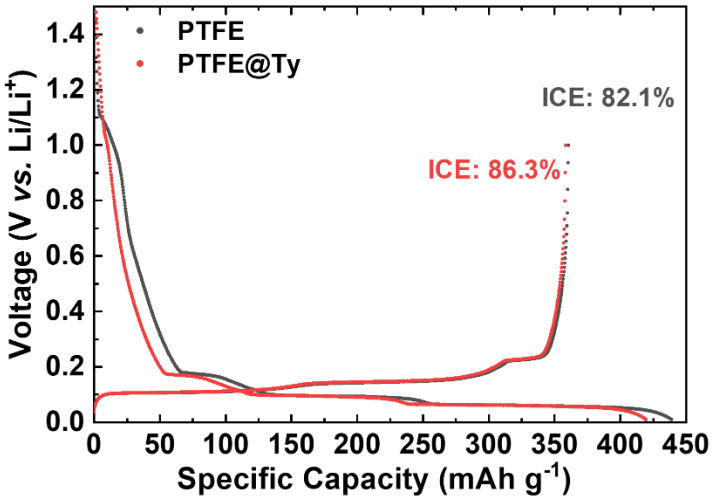

Figure S22. The first charge/discharge graph and ICE (@0.05C rate) of a half-cell electrode with an artificial graphite: CNT: PTFE: Ty compositions of 96:2:2:0 wt% for PTFE alone and 95:2:2:1 wt% for PTFE@Ty. The electrolyte consists of 1.0 M $LiPF_6$ and 0.5 M LiDFOB in a solution of EMC and FEC with a volume ratio of 3:1.

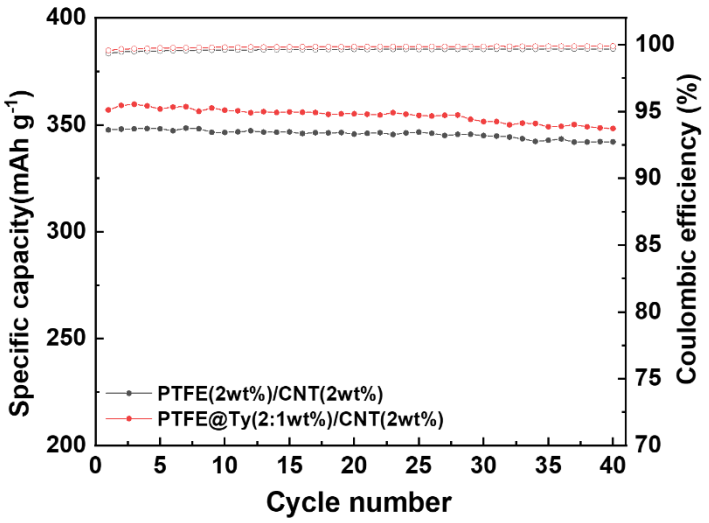

Figure S23. Cycle life of the half cells composed of artificial graphite, CNT, and PTFE mixed at a ratio of 96:2:2 wt% at a current density of 0.3C. In the case of PTFE@Ty, the ratio of artificial graphite, CNT, PTFE, and Ty is 95:2:2:1. The electrolyte consists of 1.0 M $LiPF_6$ and 0.5 M LiDFOB in a solution of EMC and FEC with a volume ratio of 3:1.

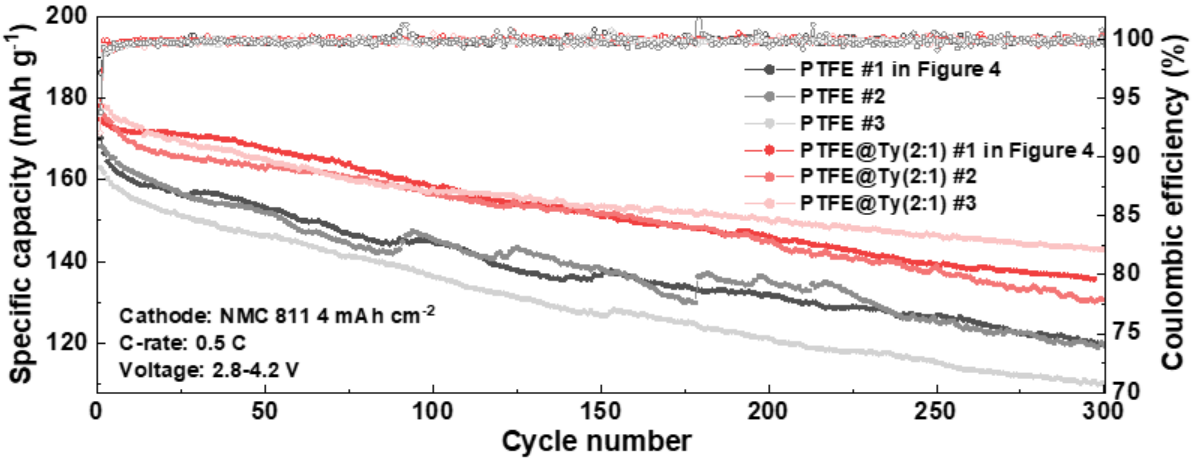

Figure S24. Reproducibility of cycling performance in full cells, as utilized in Figure 4(c).

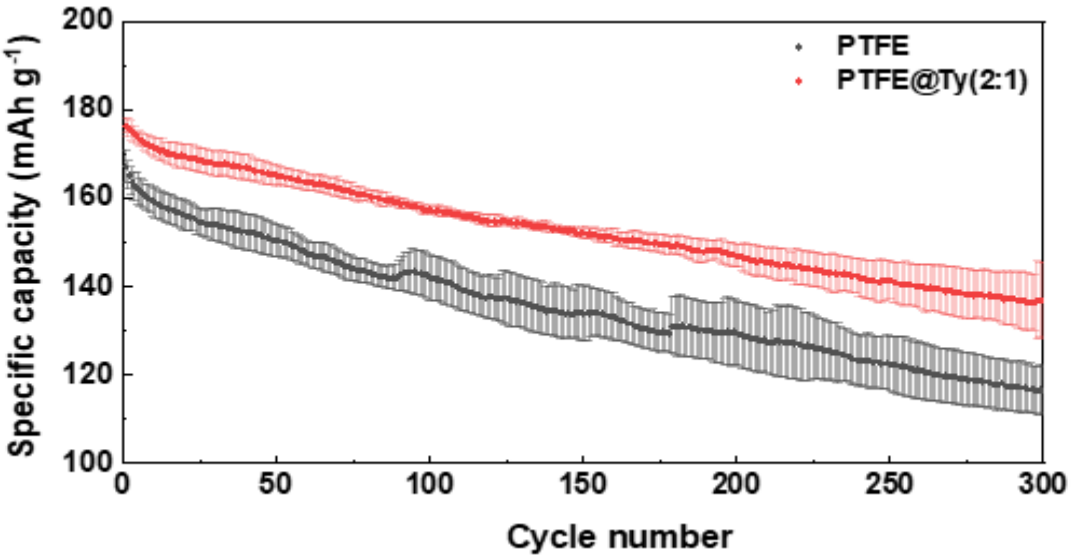

Figure S25. Statistical analysis of cycling performance of PTFE@Ty electrodes used in Figure S24 (mean ± standard deviation, n = 3).

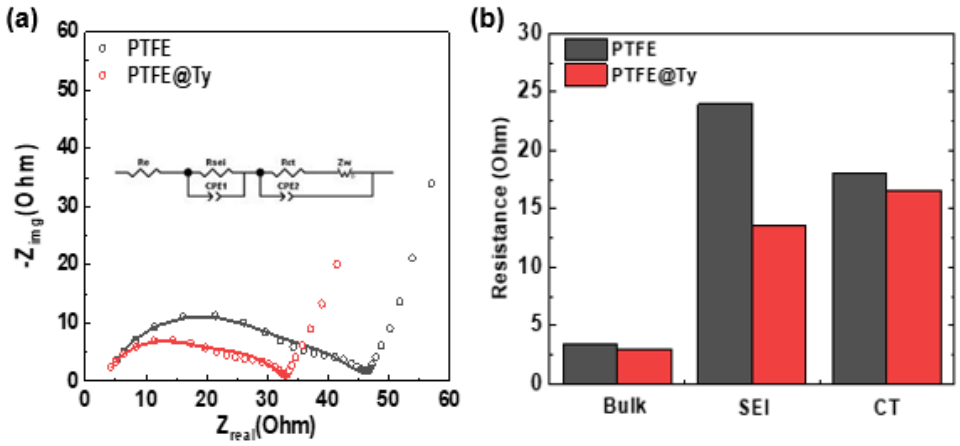

Figure S26. (a) Nyquist plots of the full cells after 150 cycles. The inset shows the equivalent circuit used for fitting; open circles represent the measured data, and solid lines correspond to the fitted data. (b) Comparison of bulk, SEI, and charge-transfer (CT) resistances extracted from the EIS fitting.

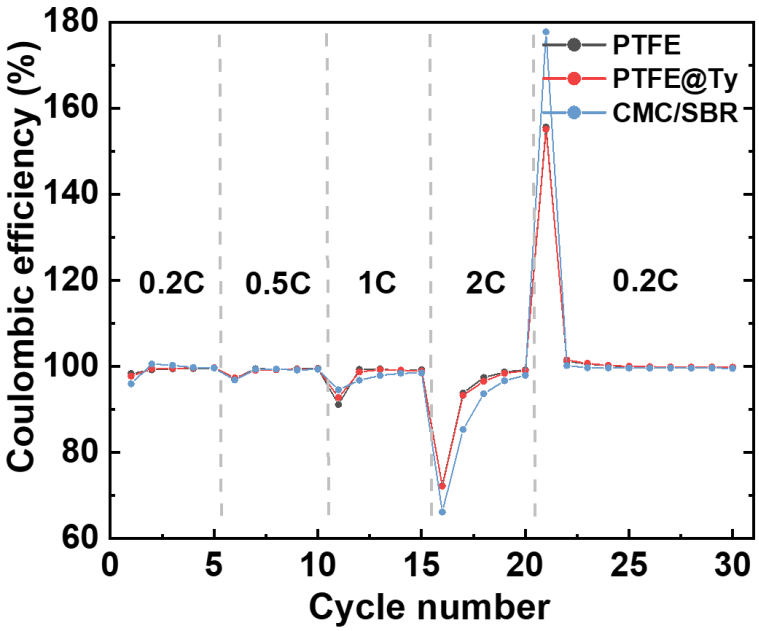

Figure S27. Coulombic efficiency of the full cell in Figure 5(a).

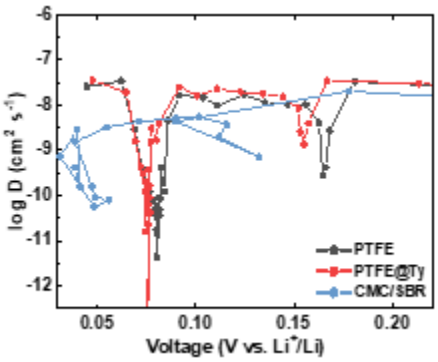

Figure S28. Additional logarithmic values of the diffusion coefficients as a function of voltage during the first lithiation process.

Table S2. The porosity was calculated using the equation $\varepsilon = 1 - \frac{m_{areal}}{L}\left(\frac{\omega_{AM}}{\rho_{AM}} + \frac{\omega_B}{\rho_B} + \frac{\omega_{CA}}{\rho_{CA}}\right)$ where m_{areal} is the areal mass loading of electrode, L is the thickness, ω is the mass fraction and ρ is density. (*7*) The subscript AM, B and CA represent active material, binder and conducting agent, respectively. The tortuosity was estimated by the formula $\tau = \frac{R_{ion}Ak\varepsilon}{2d}$ where A is surface area of electrode, k is ionic conductivity of electrolyte (4.47×10^{-3} S cm^{-1}) (*8*) and d is the electrode thickness. (*9*) The ionic resistance (R_{ion}) was calculated using the following equation, $R_t = \frac{R_{ion}}{3} + R_{HFR}$, where R_t and R_{HFR} are the total resistance and the high-frequency resistance (contact resistance). (*7, 9*) R_{HFR} can be obtained from the extrapolation of the high-frequency region, depicted as a dashed line in Figure 5(c), while the R_t value is obtained from the interception point of the dashed extrapolation line in the low-frequency region and the horizontal axis.

	CMC/SBR	**PTFE**	**PTFE@Ty**
R_t	63.8	40.2	38.2
R_{HFR}	40.2	22.7	20.1
R_{ion}	70.8	52.5	54.3
Thickness (μm)	146	143	148
Mass loading (mg cm^{-2})	21.7	22.1	22.3
Porosity (%)	32.4	29.8	31.6
Tortuosity	2.49	1.73	1.84

Table S3. Comparison with various approaches to prevent electrochemical degradation of PTFE binder in dry-processed electrodes.

Improvement methods		Remarks	ICE of anode half cell	ICE of full cell	Cathode	Rate	Capacity retention	Ref
Raising the LUMO level	Additive	Addressing intrinsic problem; Fully dry process	94.4%	82.1%	NMC 811	0.5C	77.7% after 300 cycles	This work
Blocking electron transfer	PEO coating	Wet process for coating	80.2%	79.1%	NMC 811	4C	86% after 50 cycles	(*10*)
	PEO coating	Wet process for coating	90.9%	83.7%	$LiNi_{0.75}Mn_{0.25}O_2$	0.3C	87% after 1700 cycles	(*11*)
	PVP additive	Partial protection; Fully dry process	92.4%	88.3%	NMC 811	0.2C	86.3% after 200 cycles	(*12*)
	FEC derived SEI	Limitations of choosing electrolytes; Low voltage LFP	87.2%	83.8%	LFP	0.2C	60% after 200 cycles	(*13*)
None	None	PTFE alone	77.9%	N/A	NMC 622	0.2C	74.1% after 400 cycles	(*7*)
	None	PTFE alone	88.2%	N/A	NMC 622	0.5C	72% after 300 cycles	(*3*)

Note S1. Calculation of the capacity loss due to PTFE reduction.

The theoretical specific capacity of a material can be calculated using the following general expression:

$$C_{theoritical}(mAh\ g^{-1}) = \frac{n \times F \times 1000}{3.6\ \times M}$$

where

- n = number of electrons transferred per repeating unit,
- F = Faraday constant (96,485 C mol^{-1}),
- M = molar mass of the repeating unit (g mol^{-1}),
- 3.6 = conversion factor from coulombs to mAh.

For PTFE with repeating unit C_2F_4, the full reduction reaction is:

$$4Li^+ + C_2F_4 + 4e^- \rightarrow 4LiF + 2C$$

- Molar mass of C_2F_4: M = 100.02 g mol^{-1}
- Number of electrons transferred: n = 4

Thus,

$$C_{theoritical} = \frac{4 \times 96{,}485 \times 1000}{3.6\ \times 100.02} \approx 1072\ mAh\ g^{-1}$$

Thus, the theoretical specific capacity of PTFE is 1072 mAh g^{-1} assuming complete reduction of the C_2F_4 repeating unit.

References

1. F. Neese, Wiley interdiscip. *Rev.: Comput. Mol. Sci* **2**, 73-78 (2012).

2. F. Neese, Software update: the ORCA program system, version 4.0. *Wiley Interdisciplinary Reviews: Computational Molecular Science* **8**, e1327 (2018).

3. Y. Suh, J. K. Koo, H.-j. Im, Y.-J. Kim, Astonishing performance improvements of dry-film graphite anode for reliable lithium-ion batteries. *Chemical Engineering Journal* **476**, 146299 (2023).

4. J. Lee, H. Park, J. Hwang, J. Noh, C. Yu, Delocalized lithium ion flux by solid-state electrolyte composites coupled with 3D porous nanostructures for highly stable lithium metal batteries. *ACS nano* **17**, 16020-16035 (2023).

5. E. Deiss, Spurious chemical diffusion coefficients of Li+ in electrode materials evaluated with GITT. *Electrochimica Acta* **50**, 2927-2932 (2005).

6. W. Weppner, R. A. Huggins, Determination of the kinetic parameters of mixed-conducting electrodes and application to the system Li3Sb. *Journal of The Electrochemical Society* **124**, 1569 (1977).

7. R. Tao *et al.*, High-throughput and high-performance lithium-ion batteries via dry processing. *Chemical Engineering Journal* **471**, 144300 (2023).

8. S.-J. Park, J.-Y. Hwang, C. S. Yoon, H.-G. Jung, Y.-K. Sun, Stabilization of lithium-metal batteries based on the in situ formation of a stable solid electrolyte interphase layer. *ACS Applied Materials & Interfaces* **10**, 17985-17993 (2018).

9. J. Landesfeind, J. Hattendorff, A. Ehrl, W. A. Wall, H. A. Gasteiger, Tortuosity determination of battery electrodes and separators by impedance spectroscopy. *Journal of The Electrochemical Society* **163**, A1373 (2016).

10. T. Lee *et al.*, Non-Electroconductive Polymer Coating on Graphite Mitigating Electrochemical Degradation of PTFE for a Dry-Processed Lithium-Ion Battery Anode. *ACS Applied Materials & Interfaces* **16**, 8930-8938 (2024).

11. Z. Wei *et al.*, Removing electrochemical constraints on polytetrafluoroethylene as dry-process binder for high-loading graphite anodes. *Joule* **8**, 1350-1363 (2024).

12. J. Lee *et al.*, Anode interface-stabilizing dry process employing a binary binder system for ultra-thick and durable battery electrode fabrication. *Chemical Engineering Journal* **503**, 158271 (2025).

13. S. Han *et al.*, Mitigating PTFE decomposition in ultra thick dry-processed anodes for high energy density lithium-ion batteries. *Journal of Energy Storage* **96**, 112693 (2024).